Received: 16 December 2021 | Revised: 20 January 2022 | Accepted: 20 January 2022

DOI: 10.1111/mmi.14884

RESEARCH ARTICLE

WILEY

SxsA, a novel surface protein mediating cell aggregation and adhesive biofilm formation of *Staphylococcus xylosus*

Carolin J. Schiffer[1] | **Christoph Schaudinn**[2] | **Matthias A. Ehrmann**[1] | **Rudi F. Vogel**[1]

[1]Lehrstuhl für Technische Mikrobiologie, Technische Universität München, Freising, Germany

[2]Advanced Light and Electron Microscopy, Robert Koch Institute, Berlin, Germany

Correspondence
Matthias A. Ehrmann and Carolin J. Schiffer, Lehrstuhl für Technische Mikrobiologie, Technische Universität München, Freising 85354, Germany.
Emails: matthias.ehrmann@tum.de and carolin.schiffer@tum.de

Present address
Carolin J. Schiffer and Matthias A. Ehrmann, Lehrstuhl für Mikrobiologie, Technische Universität München, Freising, Germany

Funding information
Forschungskreis der Ernährungsindustrie, Grant/Award Number: AIF19690N; German Federation of Industrial Research Associations; German Federal Ministry for Economic Affairs and Energy

Abstract

Biofilm formation of staphylococci has been an emerging field of research for many years. However, the underlying molecular mechanisms are still not fully understood and vary widely between species and strains. The aim of this study was to identify new effectors impacting biofilm formation of two *Staphylococcus xylosus* strains. We identified a novel surface protein conferring cell aggregation, adherence to abiotic surfaces, and biofilm formation. The *S. xylosus* surface protein A (SxsA) is a large protein occurring in variable sizes. It lacks sequence similarity to other staphylococcal surface proteins but shows similar structural domain organization and functional features. Upon deletion of *sxs*A, adherence of *S. xylosus* strain TMW 2.1523 to abiotic surfaces was completely abolished and significantly reduced in TMW 2.1023. Macro- and microscopic aggregation assays further showed that TMW 2.1523 *sxsA* mutants exhibit reduced cell aggregation compared with the wildtype. Comparative genomic analysis revealed that *sxs*A is part of the core genome of *S. xylosus*, *Staphylococcus paraxylosus*, and *Staphylococcus nepalensis* and additionally encoded in a small group of *Staphylococcus cohnii* and *Staphylococcus saprophyticus* strains. This study provides insights into protein-mediated biofilm formation of *S. xylosus* and identifies a new cell wall-associated protein influencing cell aggregation and biofilm formation.

KEYWORDS
amyloids, autoaggregation, biofilm, *Staphylococcus xylosus*

1 | INTRODUCTION

Staphylococcus xylosus, first described by Schleifer and Kloos (1975), belongs to the large group of coagulase-negative staphylococci (CNS). It is commonly used as a starter organism in raw sausage fermentations where its ability to reduce nitrate and its contribution to aroma formation is of high technological value (Leroy et al., 2006). Yet, CNS are also ubiquitous commensals of mammal skin and have been considered opportunistic pathogens in humans and animals (Becker et al., 2014; Michels et al., 2021). In this context, *S. xylosus* has been repeatedly associated with bovine mastitis infections (de Buck et al., 2021; Supré et al., 2011). Colonization of surfaces and biofilm formation play an important role during infections as they increase a bacterium's tolerance to host defense mechanisms and antibacterial treatments (Foster et al., 2014; Otto, 2008; Schilcher & Horswill, 2020). Biofilm formation of bacteria is a multifactorial process, often enabled by more than one mechanism. It can vary between and within bacterial species as well as it is strongly affected by environmental factors and physical conditions (Karatan & Watnick, 2009; Lawal et al., 2021; Schiffer et al., 2019). While the

understanding of molecular mechanisms, regulatory systems, and genes involved in biofilm formation processes is still growing, studies on the composition of biofilm matrices revealed that the extracellular matrix, in which the cells are embedded, is usually composed of three major constituents: polysaccharides, extracellular DNA, and proteins with lipids being involved occasionally as well (Schilcher & Horswill, 2020).

The role of proteins in biofilm formation of staphylococci is currently most widely studied in *Staphylococcus aureus* and *Staphylococcus epidermidis*. Next to secreted proteins, such as the 18 kDa small basic protein (Sbp) (Decker et al., 2015) and the extracellular adherence protein (Eap) (Yonemoto et al., 2019), cell wall-anchored proteins play a major role in the biofilm formation process. They either mediate primary attachment to surfaces and/or cell accumulation at later stages of the biofilm maturation phase (Foster, 2019; Speziale et al., 2014). Most of them comprise a C-terminal LPxTG cell wall-anchoring motif, which covalently binds them to peptidoglycan by a sortase-mediated mechanism, and an N-terminal YSIRK-G/S signal peptide, which is supposed to translocate proteins to the cross wall (Bowden et al., 2002; DeDent et al., 2008). During primary attachment of staphylococcal cells to biotic surfaces, microbial surface components recognizing matrix molecules (MSCRAMMs) that bind to host factors such as fibronectin (FnBpA, FnBpB, Embp), fibrinogen (ClfA, ClfB), and collagen (Cna, SdrF) play an essential role (Foster, 2020; Foster et al., 2014). Proteins such as autolysins and the biofilm-associated protein (Bap) on the other hand mediate attachment to abiotic surfaces (Cucarella et al., 2001; Heilmann et al., 1997). During subsequent biofilm accumulation, proteins usually contribute to cell aggregation either by interacting with surface structures on neighboring cells or by the formation of amyloid fibers (Speziale et al., 2014; Taglialegna, Lasa, et al., 2016a). Examples for staphylococcal proteins conferring biofilm accumulation include Bap and the accumulation-associated protein Aap (Rohde et al., 2005; Taglialegna, Navarro, et al., 2016b). The function of Bap is especially well characterized in *S. aureus* strain V329 and was found to be based on amyloid assembly of N-terminal peptides upon extracellular processing under acidic conditions and low Ca^{2+} concentrations (Taglialegna, Navarro, et al., 2016b). Aap of *S. epidermidis* and its homolog, *S. aureus* surface protein G (SasG), undergo extracellular proteolytic cleavage as well, resulting in different versions of truncated isoforms of the protein (Rahmdel & Götz, 2021). In the isoforms, G5-E domains of the B region are exposed and mediate intercellular adhesion in a Zn^{2+}-dependent matter (Geoghegan et al., 2010; Yarawsky et al., 2020).

Only a few studies have addressed adhesion mechanisms and biofilm matrix composition in coagulase-negative staphylococci (CNS), other than *S. epidermidis* in the past. We have previously reported that biofilm-producing *S. xylosus* strains do not encode an Aap/SasG homolog in their genome as well as that Bap is only of minor importance in biofilm formation of *S. xylosus* (Schiffer et al., 2019; Schiffer et al., 2021). We, therefore, postulate that another mechanism must be responsible for protein-mediated cell aggregation and biofilm formation in this species. In the following, we identify and characterize a new protein, influencing multicellular behavior and surface adhesion of *S. xylosus*.

2 | MATERIALS AND METHODS

2.1 | Bacterial strains and growth conditions

Staphylococcus xylosus TMW 2.1023 and TMW 2.1523 and their respective *bap*-deficient mutants are biofilm-positive strains that have been described in previous studies before (Schiffer et al., 2019; Schiffer et al., 2021). *Escherichia* (*E.*) *coli* DC10B, a cytosine methyltransferase-negative derivate of *E. coli* DH10B (Monk et al., 2012), was used for vector assembly, propagation, and purification. *E. coli* was grown in Lysogeny Broth (LB, tryptone 10 g/L, yeast extract 5 g/L, NaCl 5 g/L) at 28 and 37°C, respectively. *S. xylosus* was cultured in Trypticase soy broth (casein peptone 15 g/L, soy peptone 15 g/L, yeast extract 3 g/L, pH 7.2) which was supplemented with either no glucose (TSB_N), 1% glucose (TSB^+), or 1% glucose with additional acidification to pH 6 using either 80% lactic acid (Lac^+) or 6 N HCl (TSB^+-HCl). For transformation experiments, *S. xylosus* was cultivated in basic medium (BM, 1% peptone, 0.5% yeast extract, 0.5% NaCl, 0.1% glucose, 0.1% K_2HPO_4, pH 7.2) and brain heart infusion (BHI) broth. When necessary, 20 μg/ml (*E. coli*) or 10 μg/ml (staphylococci) of chloramphenicol (CarlRoth) was added to the respective growth medium.

2.2 | Generation of mutant strains by allelic replacement

For mutagenesis of the chromosomal *sxs*A gene in *S. xylosus*, regions up- and downstream of the to be deleted sequence (1376 nt deletion in N-terminal part of the protein) were amplified using primers *sxs*A1F (5′-TGTACTGCAGGATATAGCTGAAGTTCCTCC-3′) and *sxs*A2R (5′-GTTCCACTGTCTGGTCTAGCTCATAGCTGTCTACTTCTC-3′) as well as *sxs*A3F (5′-GAGAAGTAGACAGCTATGAGCTAGACCAGACAGTGGAAC-3′) and *sxs*A4R (5′- TCAGCTCGAGGTTCACACTATCTGGTACATC-3′). Introduced restriction sites for cloning are shown underlined. All primer sequences were chosen based on the criteria that they match the target sequence in both *S. xylosus* strains (TMW 2.1023, TMW 2.1523); thus, they were designed to map on conserved regions of the protein. The two obtained PCR products were purified using a Monarch PCR and DNA cleanup kit (New England Biolabs), and primers *sxs*A1F and *sxs*A4R were used for subsequent overamplification to generate the vector insert. Restriction digest of insert and vector using PstI-HF and XhoI-HF (NEB) followed and the insert was ligated (T4 DNA Ligase, Thermo Fisher Scientific) into the shuttle vector pIMAY* (Schuster et al., 2019). The construct was transformed into the *dcm*-negative *E. coli* strain DC10B by electroporation. Successful transformants were selected on chloramphenicol (10 μg/ml) plates. The plasmid was isolated using the Monarch plasmid DNA miniprep kit (NEB), sequenced to confirm correct assembly, and transformed

into electrocompetent *S. xylosus* cells as previously described (Monk & Stinear, 2021; Schiffer et al., 2021). Hereby, the transformation of wildtype strains was performed to obtain Δ*sxs*A mutants, as well as *bap*-deficient mutants (Schiffer et al., 2021) were transformed, to generate Δ*bap*Δ*sxs*A mutant strains. In the end, successful gene deletion and allelic replacement of the *sxs*A sequence as well as loss of pIMAY* were verified by colony PCR using primers *sxs*A1F and *sxs*A4R. Loss of chloramphenicol resistance was verified by replica plating.

2.3 | Biofilm formation and adherence to surfaces

For quantification of biofilm formation on abiotic surfaces, a 96-well plate assay based on safranin-O staining of adherent cells was used as described by Schiffer et al. (2019). Therefore, strains were cultured in different media (TSB_N, TSB^+, Lac^+) and on different supports (hydrophobic [Sarstedt], hydrophilic [Nunclon™ delta, Thermo Scientific]) for 24 h at 37°C. Adherent cells were subsequently stained with 0.1% safranin-O, and biofilm was quantified by determining the absorbance at 490 nm in a microplate reader ($Spectrostar^{Nano}$, BMG Labtech). For visualization purposes, cells were also cultured in Nucleon™ Delta-treated culture dishes (Thermo Scientific), stained the same way, and photographed. To test the impact of calcium and its respective chelating agent on biofilm formation either $CaCl_2$ (20 mM) and/or EDTA (0.2 mM) were added to the wells (Sarstedt 96-well plate) at the beginning of the incubation period. dH_2O served as the respective control. Cytotoxicity of the reagents was excluded by incubating cells overnight with/without the mentioned reagents in TSB_N and confirming similar growth by OD_{600} measurement after 24 h.

2.4 | Aggregation assays in suspension

For determination of differences in cellular aggregation, wildtype and Δ*sxs*A strains were cultivated in 50 ml of either TSB_N or TSB^+ in Erlenmeyer flasks for up to 24 h at 37°C and 200 rpm. They were removed from the shaker after 12 and 24 h, respectively, and cell aggregation was recorded visually as well as pictures were taken immediately.

To record sedimentation over time, wildtype, Δ*bap*, Δ*sxs*A, and Δ*bap*, *sxs*A strains were grown in TSB_N (37°C, 200 rpm) for 16 h and 3 ml of the cell suspension was transferred to a culture tube. Tubes remained in a steady position and pictures were taken to record cell sedimentation at time zero (t_0) and after one (t_1), two (t_2), five (t_5), and 24 (t_{24}) h, respectively.

2.5 | Colony morphology on congo red agar

Colony morphology on congo red agar (CRA) was examined for wildtype and mutant strains. Minor modifications to the protocol described in Schiffer et al. (2021) were made, since this time, CRA plates contained no glucose and were simply composed of 15 g/L casein peptone, 5 g/L soya peptone, 5 g/L NaCl, 15 g/L agar, 0.8 g/L congo red, and pH 7.2. Strains were streaked out, plates were incubated at 37°C for 24 h and remained at room temperature for another 2 days before they were visually examined. Congo red is known to interact with proteinaceous and amyloidogenic structures; red, dry, and rough colony morphologies can be considered an indicator for microbial-generated amyloid fibers (Erskine et al., 2018).

2.6 | Growth dynamics

Growth dynamics were recorded for wildtype and mutant strains in TSB_N, TSB^+, Lac^+, and TSB^+-HCl over a period of 33 h at 37°C in a microplate reader ($Spectrostar^{Nano}$, BMG Labtech). Therefore, overnight cultures of the respective strains were washed and diluted to an OD_{600} of 0.1 in the respective growth medium. Two hundred microliters of the cell suspensions were transferred to each well of a 96-well plate (Sarstedt). Growth was monitored by measuring the absorbance at 600 nm every 30 min. Before each measurement, the plate was shaken for 10 min at 600 rpm. All data were recorded in technical and biological triplicates. When necessary, colony-forming units per ml were determined by serial dilution in Ringer's solution and plating on TSA.

2.7 | SDS-PAGE analysis of whole-cell protein extracts

SDS-PAGE analysis of whole-cell protein extracts was performed as described by Schiffer et al. (2021). Basically, cells were grown in TSB_N until the early stationary phase. Five milliliters of cell suspension were harvested, washed, and lysed in an isosmotic digestion buffer (150 µl PBS + 30% [wt/vol] raffinose [Sigma], 7 µl lysostaphin [1 mg/ml, Sigma], and 3 µl DNAseI [1 mg/ml, Sigma]) at 37°C for 2 h. In the following, protoplasts were sedimented at 8000 x *g* for 30 min (slow deceleration) and supernatants were subjected to SDS-PAGE analysis (10% resolving gel, 4% stacking gel). Protein staining was performed using ROTI®Blue (CarlRoth) according to the manufacturer's instructions.

2.8 | CLSM imaging

Overnight cultures of wildtype and mutant strains were diluted (1:5 vol/vol) with TSB_N, of which 2.5 ml were transferred to ibidi dishes with glass bottom (ibidi GmbH). After incubation for 16 h at 37°C with 150 rpm, the cultures were stained with Syto60 (DNA, final concentration 5 µM) and Thioflavin T (amyloids, final concentration 20 µM) for 30 min in the dark and imaged in the CLSM (LSM 780, Carl Zeiss Microscopy).

2.9 | SEM imaging

Overnight cultures of wildtype and mutant strains were diluted (1:5 vol/vol) with TSB_N, of which 2.5 ml were transferred to the wells

of 12 well plates containing a porous glass bead each (ROBU®, VitraPOR®, Porous Glass Bead, 4.0 mm, 60 μm pore size). After incubation for 16 h at 37°C with 150 rpm the cultures were fixed (4% paraformaldehyde, 2.5% glutaraldehyde in 50 mM HEPES, pH 7.0) for 24 h, dehydrated in a graded ethanol line (30%, 50%, 70%, 90%, 95%, 100%, 100%) chemically dried (hexamethyldisilazane) overnight, mounted on aluminum stubs, sputter-coated with a 12 nm gold–palladium layer, and imaged in the SEM (ZEISS 1530 Gemini, Carl Zeiss Microscopy GmbH) operating at 3 kV and using the in-lens secondary electron detector.

2.10 | TEM imaging

Overnight cultures of wildtype and mutant strains were diluted (1:5 vol/vol) with TSB_N, of which 5 ml were transferred to 50 ml centrifugation tubes. After incubation for 16 h at 37°C at 150 rpm, the supernatant of the cultures was negatively stained with 0.5% uranyl acetate and imaged in the TEM (Tecnai 12 Spirit; FEI) at an acceleration voltage of 120 kV).

2.11 | Full proteome analysis

For confirmation of successful mutant strain generation and information on the expression of SxsA under different growth conditions, full proteome analysis was performed as described by Schiffer et al. (2021). The proteomics data set is accessible via ProteomeXchange using the identifier PXD029728.

2.12 | Bioinformatics and statistical analysis

General sequence analysis, comparisons, alignments, and phylogenetic trees were calculated using CLC Main Workbench 8 (CLC bio); for alignments, the integrated ClustalO plugin was used. EF-hand motifs (Lewit-Bentley & Réty, 2000) were predicted using ProScan (Prosite database) with a cutoff set to 80% similarity. Coiled-coil motifs were predicted using MARCOIL (Delorenzi & Speed, 2002) and confirmed with the overview generated by the MPI bioinformatics toolkit (Gabler et al., 2020). Amyloid-prone regions and peptides were identified by comparing the results generated by four different algorithms WALTZ-DB 2.0 (Louros et al., 2020), AGGRESCAN (de Groot et al., 2012), TANGO (Fernandez-Escamilla et al., 2004), and FoldAmyloid (Garbuzynskiy et al., 2010). Molecular weight (Mw) and isoelectric point (pI) were computed by the respective tool available on the Expasy server (https://web.expasy.org/compute_pi/). Genomes were screened for proteins harboring a C-terminal LPxTG cell wall-anchored motif using the respective Prosite algorithm, [LY]PX[TSA][GNAST]X(0,10){DEQNKRP}{DEQNKRP}{DEQNKRP}{DEQNKRP}{DEQNKRP}{DEQNKRP}{DEQNKRP}{DEQNKRP}{DEQNKRP}X(0,15)[DEQNKRH]X(0,5) (Roche et al., 2003). Signal peptides and hydrophobic transmembrane segments were predicted by InterPro (86.0). NCBI BLASTP searches against the protein database were used for the analysis of sequence similarities to other proteins, identification of potential homologs and to estimate the prevalence of *sxs*A within the species *S. xylosus* as well as other staphylococcal species. Genomes were screened for the presence of genetic islands using island viewer 4 (Bertelli et al., 2017). Whole-genome sequencing data of TMW 2.1023 and TMW 2.1523 have been deposited at GenBank under the accession nos. JAEMUG000000000 and CP066721-CP066725, respectively. All further *sxs*A sequences included in the analysis are available on NCBI under the indicated Locustag (Table S5). All experiments were performed in biological triplicates and data are presented as mean ± standard errors of the means, unless stated otherwise. SigmaPlot Version 12.5 (Systat Software GmbH) was used to perform Student's *t* tests.

3 | RESULTS

3.1 | Presence of YSIRK-G/S and LPxTG motif-containing proteins in the genomes of *S. xylosus* strains TMW 2.1023 and TMW 2.1523

Since surface proteins are known to be essential in adherence and biofilm formation of other coagulase-negative staphylococci (Foster, 2020; Foster et al., 2014), we have screened the genomic sequences of two *S. xylosus* strains (TMW 2.1023 and TMW 2.1523) for open-reading frames (ORFs) encoding surface proteins that could act as Bap alternatives mediating biofilm formation in this organism. Special emphasis was laid on the presence of an N-terminal YSIRK-G/S signal peptide, a C-terminal LPxTG cell wall-anchoring motif, and a hydrophobic transmembrane segment, as most surface proteins involved in biofilm formation described for other staphylococci share these motifs (Bowden et al., 2002; Mazmanian et al., 2001). Table 1 shows an overview of potential candidate proteins, which were identified in the genomes of the respective *S. xylosus* strains. All protein sequences were further subjected to the InterPro functional analysis tool, to screen for enzymatic domains, as such functional domains are commonly identified in YSIRK-G/S containing surface proteins of streptococci (Bai et al., 2020). Proteins with hydrolytic domains were excluded from further analyses as we were rather concentrating on large structural proteins. Besides Bap, a protein encoded in both *S. xylosus* strains, TMW 2.1023 (JGY91_02365) and TMW 2.1523 (JGY88_01050), and another one encoded in TMW 2.1023 only (JGY91_13535/13480) remained particularly interesting, as they comprise both motifs (YSIRK-G/S, LPxTG), thus are present on the cell surface, display no enzymatic domains, and are very large. We followed the nomenclature proposed by Mazmanian et al. (2001) for staphylococcal surface proteins and therefore named them *Staphylococcus xylosus* surface protein A (SxsA) and B (SxsB). Of note is that while *sxs*A is chromosomally encoded in both strains,

TABLE 1 Proteins of *S. xylosus* TMW 2.1023 and TMW 2.1523 harboring a YSIRK-G/S signal peptide and/or an LPxTG cell wall-anchored motif

TMW 2.1023				TMW 2.1523				
Locustag	**size (aa)**	**YSIRK**	**LPxTG**	**Locustag**	**size (aa)**	**YSIRK**	**LPxTG**	**Note**
JGY91_00380	757	YSIRK	–	JGY88_12550	721	YSIRK	–	AB hydrolase
JGY91_01665	748	YSIRK	–	–				AB hydrolase
JGY91_02365	2044	YSIRK	LPNTG	JGY88_01050	3123	YSIRK	LPNAG	SxsA
JGY91_02455	1651	YSIRK	LPETG	JGY88_01140/45	2161	YSIRK	LPETG	Bap
*JGY91_04265-70	–	FSIRK		–				AB hydrolase
JGY91_13535/ 13480^{P}	1187	FSIRK	LPNTG	–				SxsB
JGY91_12735	648	–	LPNTG	JGY88_11760	884	–	LPNTG	Fibrinogen-binding adhesin
JGY91_13335^{P}	654	–	LPDTG	JGY88_13950^{P}	654	–	LPDTG	Albumin-binding domain (GA module)
				JGY88_00260	659	-	LPDTG	

Note: Asterisk indicates truncated frames due to an internal stop, P indicates sequences that are encoded on plasmids. Some sequences are split into two different contigs in the WGS data set, however, PCR analysis confirmed their entirety as one single ORF. The last column indicates whether enzymatic domains were predicted from sequence analysis or if the protein has been described/named already.

*sxs*B is carried on a plasmid in strain TMW 2.1023 only. Additionally, we consulted the proteomic data set, we obtained from previous work (Schiffer et al., 2021) and found that SxsA shows similar intensity value changes as Bap, namely higher detectable amounts under planktonic compared with sessile growth conditions as well as higher detectable amounts when cells were grown in a neutral medium without glucose (TSB_N), in contrast to when cells were grown in glucose-containing medium additionally acidified to pH 6 by lactic acid (Lac^+). For a more detailed overview of the intensity levels determined by full proteome analysis, see Table S1.

For further investigations, we selected SxsA as a promising candidate to prove our hypothesis that another surface protein than Bap might be involved in biofilm formation of *S. xylosus*.

3.2 | Mutagenesis of the chromosomal *sxs*A gene

*Sxs*A-mutant strains (Δ*sxs*A) were generated for both *S. xylosus* strains. Furthermore, double mutants, deficient in *bap* as well as *sxs*A (Δ*bap*, *sxs*A), were also included in the project. SDS-PAGE analysis was performed to confirm the successful deletion of the respective genes. As we have already reported in Schiffer et al. (2021), Bap is hardly detectable on SDS-PAGE. SxsA, however, is visible as a distinct band at the expected size with 223 kDa for TMW 2.1023 and 338 kDa for TMW 2.1523, respectively. The band was not detectable in mutant strains as shown in Figure 1. It is highly likely that the detected band corresponds to SxsA rather than that expression of another protein decreases upon *sxs*A deletion, as in silico prediction of protein masses of proteins encoded by the two *S. xylosus* strains did not predict any other protein running at the expected size (Table S2). Yet, to confirm the results predicted by the gels, a full proteome analysis was performed. With very few exceptions that are considered as artifacts, no peptides mapping on SxsA were found in the mutant samples, confirming successful deletion of *sxs*A in both *S. xylosus* strains (Tables S3 and S4).

3.3 | Optical density-based growth curves differ between WT and mutant

To exclude that any major growth defects resulted from the transformation procedure or were caused by deleting *sxs*A, growth curves were recorded in a microtiter plate-based format over a period of 33 h. Growth curves confirmed that mutant strains mostly showed a similar growth behavior compared with their respective wildtype strains (Figure S1). Only TMW 2.1523 Δ*sxs*A strains displayed different growth dynamics, in particular, growth rates increased faster, and higher maxima ODs were obtained in some media (TSB^+, Lac^+) for mutant in contrast to wildtype strains. The measured differences in OD between wildtype and mutant strains presumably reflect different cell aggregation behaviors and are probably enhanced by the conditions of the format used (weak aeration and insufficient shaking in the microplate assay). This is also supported by data indicating

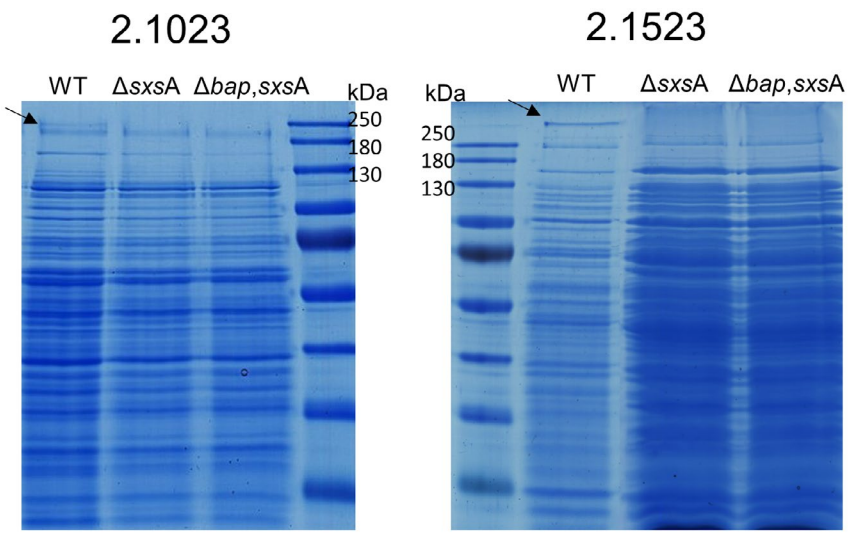

FIGURE 1 SDS-PAGE analysis of wildtype and *sxs*A-mutant strains. The arrow points to the band corresponding to SxsA (TMW 2.1023: 223 kDa, TMW 2.1523: 338 kDa)

that the difference is almost eliminated when cells are grown in the Erlenmeyer flasks under vigorous agitation (compare Section 3.5). Furthermore, almost the same high values of colony-forming units (cfu) were determined after incubation in TSB^+ for 24 h for TMW 2.1523 wildtype and Δ*sxs*A strain resulting in values of 3.4 x 10^7 and 3.5 x 10^7 cfu/ml, respectively.

3.4 | Biofilm formation on abiotic surfaces is impaired in *sxs*A mutants

Biofilm formation was quantified using a 96-well assay, based on safranin-O staining of adherent cells. Deletion of *sxs*A resulted in a complete loss of the ability to form an adherent biofilm of strain TMW 2.1523 as shown in Figure 2. Differences in staining intensities of adherent cells are also visualized in Figure S2. The effect of reduced adherence of mutant strains was regardless of the growth media (TSB_N, TSB^+, Lac^+) and the support (hydrophobic and hydrophilic) used during the experiments. In contrast to TMW 2.1523, TMW 2.1023 only showed a reduction in adherence which was especially apparent in TSB_N and TSB^+ on hydrophilic support. In summary, *sxs*A deletion has an impact on adherence and biofilm formation of *S. xylosus* on abiotic surfaces, yet, strain-specific differences occur, as the impact is much larger in strain TMW 2.1523 than in strain 2.1023. No significant additional decrease in adherence was observed in double mutants (Δ*bap*, Δ*sxs*A) compared with single mutants (Δ*sxs*A).

3.5 | *sxs*A mutants show reduced intercellular adhesion and decelerated sedimentation over time

Biofilm formation and cell aggregation are often linked closely together. To see whether SxsA impacts both phenotypes, cells were grown under shaking conditions in TSB_N until they reached stationary phase (24 h) and subsequently transferred to test tubes to allow them to settle. Figure 3 shows the sedimentation state of TMW 2.1523 at different time points. A clear difference in cell aggregation is detectable between wildtype and mutant strains. While cells of wildtype strain TMW 2.1523 had already settled to the bottom of the tubes after 1 h, *bap* mutants remained in suspension until phase separation was visible after approximately 5 h. *Sxs*A mutants had not even fully settled after 24 h. The difference in cell aggregation in liquid cultures between TMW 2.1523 wildtype and the *sxs*A-deficient strain was also very distinct when cells were grown under shaking conditions in a glucose-supplemented medium (TSB^+, Figure 4a). While wildtype cells of TMW 2.1523 form visible aggregates, especially in TSB^+, only little cell aggregation is visible for the *sxs*A-deficient mutant. However, noteworthy is that the effect demonstrated in Figure 4 between heavily clumping wildtype and little clumping-mutant strains is especially prominent during exponential and early stationary growth phase. TMW 2.1523 *sxs*A mutants grown in TSB^+ start to form visible aggregates after approximately 16 h of growth as well, at a time where they have already entered stationary phase and no pH changes occur anymore. The effect of belated visible aggregation of the *sxs*A mutant is much stronger when cells are grown in glucose-supplemented media, compared with TSB_N. The enhanced aggregation is probably pH dependent since the pH is decreasing to a larger extent when cells are grown in TSB^+ compared with TSB_N (Figure 4b). Attempts to induce visible cell aggregation the opposite way, by incubating TMW 2.1523 in a strongly basic medium (TSB_N, pH 8.5), remained unsuccessful, no differences to TSB_N were observed.

The described differences between wildtype and *sxs*A mutants in cell aggregation and settling pace could not be observed to this extent for TMW 2.1023. In general, this strain showed much less cell aggregation compared with TMW 2.1523. Clumping was only detectable, when cells were incubated in TSB^+, however, compared with the heavy aggregating cells of TMW 2.1523, the multicellular effect observed for TMW 2.1023 was much smaller (see Figures S3 and S4). To sum it up, *sxs*A impacts the multicellular behavior of *S. xylosus*. Yet, strain-specific differences should be considered environmental influences.

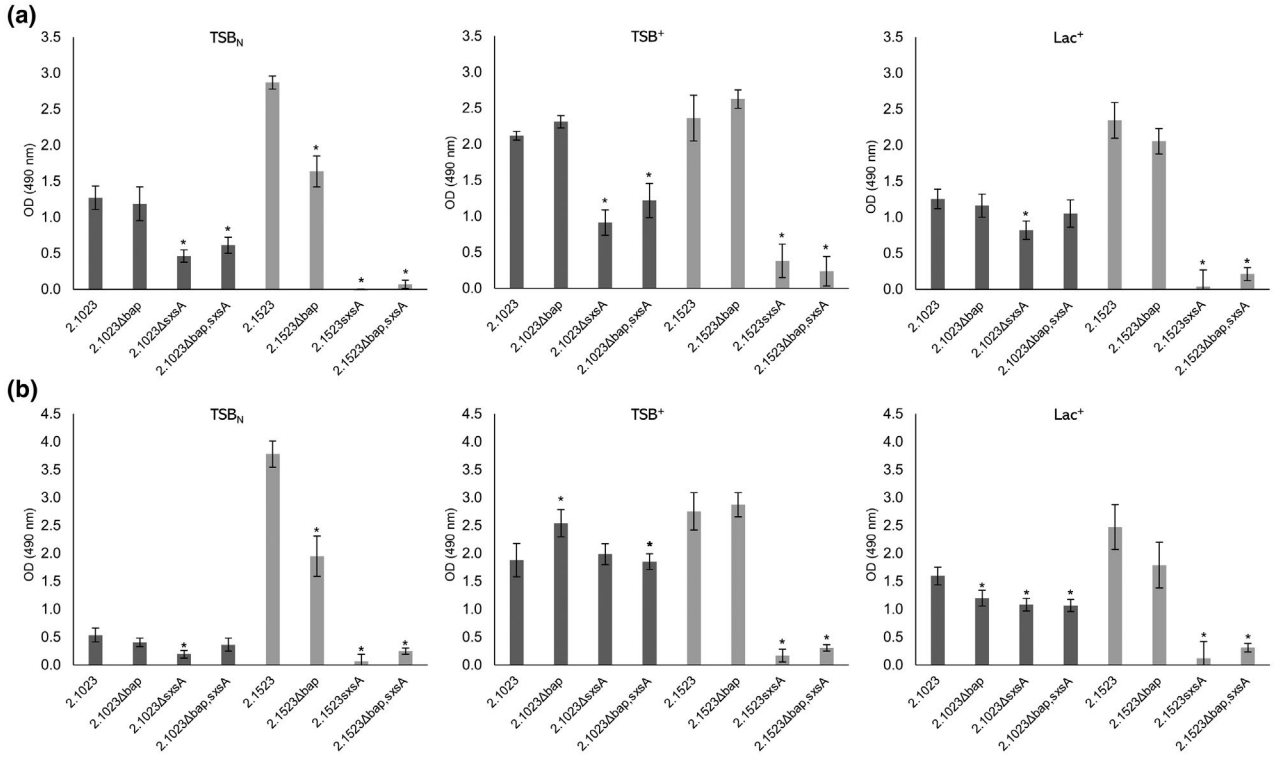

FIGURE 2 Biofilm formation of wildtype and mutant strains under different environmental conditions. Biofilm formation was quantified in a 96-well assay on hydrophilic (a) and hydrophobic (b) support in three different growth media (TSB_N, TSB^+, and Lac^+). Bars are shown as the mean of at least three independent measurements ± SE. Differences between mutant and wildtype strains that can be considered as statistically significant ($\alpha = 0.05$) are marked with asterisks (*)

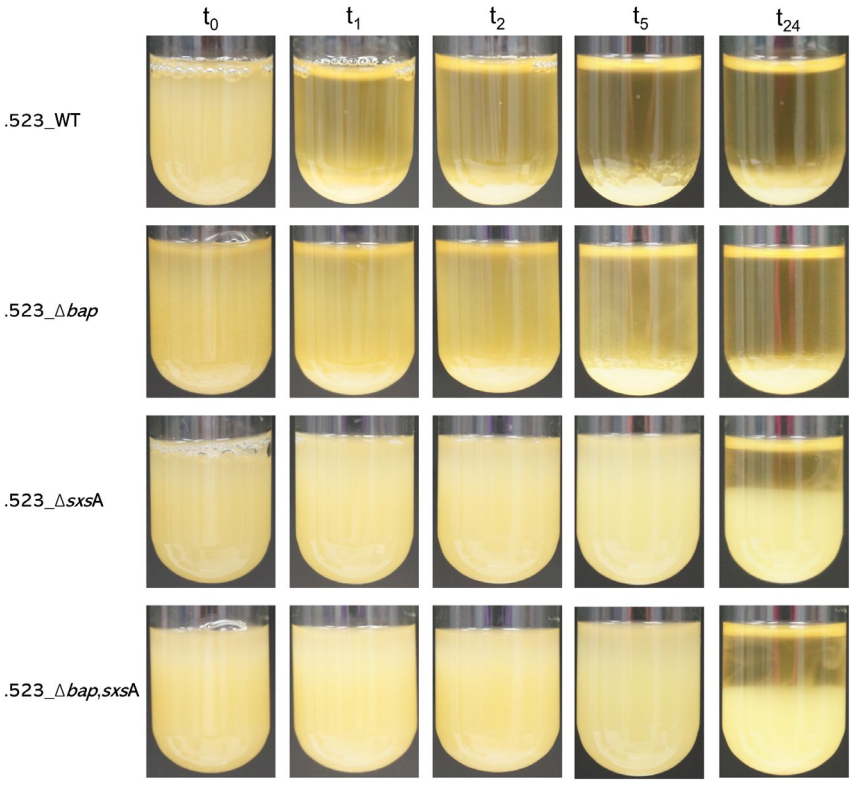

FIGURE 3 Cell sedimentation assay. Three milliliters of TMW 2.1523 cell suspensions (wildtype and mutant strains, stationary phase, TSB_N) were allowed to settle in test tubes, and pictures were taken at different time points (t_0–t_{24}). The pace of cell settlement is used as an indicator for intercellular adhesion

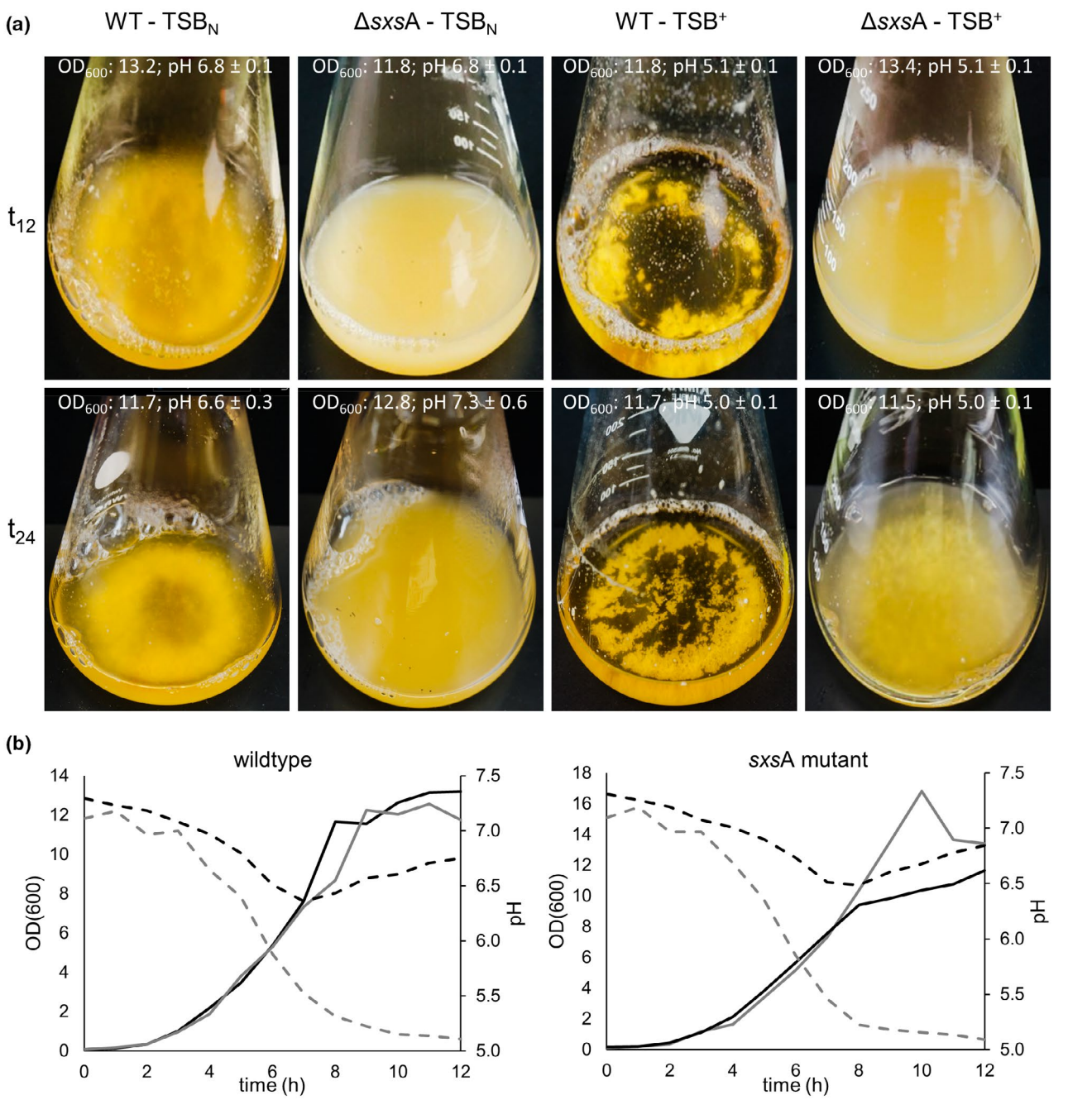

FIGURE 4 Aggregation behavior of planktonically grown wildtype and *sxs*A-mutant strains. (a) Aggregation of planktonically grown cells (TMW 2.1523 wildtype and *sxs*A mutant, 37°C, 200 rpm) was recorded after 12 and 24 h in two different growth media (TSB$_N$ and TSB$^+$). (b) Growth and pH dynamics (dashed lines) of the cultures shown in A in ●TSB$_N$ and ● TSB$^+$

3.6 | Colony morphology on congo red agar plates

Over the past years, many authors have suggested that amyloid-like fiber formation of surface proteins is a general mechanism of biofilm formation in staphylococci (Foster, 2020; Taglialegna, Lasa, et al., 2016a). Congo red (CR) dye is known to interact with amyloid structures which often leads to colony morphology changes to a red, dry, rough phenotype on CRA plates (Cucarella et al., 2001; Erskine et al., 2018). Even though CR is insufficient to confirm the presence of amyloid structures alone, as it may bind to other polymeric substances as well, it can still be a useful first indicator to see whether differences in colony morphology exist. We have previously reported that no changes in colony morphology are noticeable on CRA when the medium is supplemented with glucose (Schiffer et al., 2021). Colonies appeared black, shiny, and with smooth colony margins. In this study, we investigated colony morphologies on CRA containing no glucose. Due to the lack of glucose, the pH of the plates will not decrease during cell growth. Therefore, no changes to a darker colony color were observed on nonglucose-containing CRA plates, instead, colonies all turned red as shown in Figure S5.

While once more no differences were observable for strain TMW 2.1023, which displays in each version a red colony morphology with similar irregular, wavy colony margins, differences regarding the colony margin were noticeable between wildtype and mutant of TMW 2.1523. Again, all colonies bound the dye as well, thus appearing as red; wildtype colonies, however, showed irregular margins, while in *sxs*A mutants (Δ*sxs*A, Δ*bap*,*sxs*A), colony margins remained mostly smooth. A dry, crystalline colony consistency as reported in other studies (Cucarella et al., 2001) for *S. aureus* was not detected in the selected *S. xylosus* strains and their mutants.

3.7 | Prevalence of *sxs*A among staphylococcal species

Neither when blasting the entire SxsA sequence against the NCBI database nor when blasting parts of the protein separately, any sequence similarities to other hitherto described surface proteins (non-*sxs*A orthologs) of *S. aureus* and other staphylococci were found. Pairwise sequence comparison of SxsA and representative, well-known biofilm-associated proteins is provided in Figure S6. It confirms again that SxsA displays little homology (<10%) to other surface proteins. The BLAST-based analysis furthermore revealed that *sxs*A is likely part of the core genome of the species *S. xylosus*, *Staphylococcus pseudoxylosus*, and *Staphylococcus nepalensis* (around 60% aa identity of *S. xylosus* SxsA to other species SxsA according to BLASTp). Yet, it should be kept in mind that only limited genomic data are available on NCBI for *S. pseudoxylosus* and *S. nepalensis*, thus the data pool is limited. Other BLAST hits corresponded occasionally to genome sequences of *Staphylococcus saprophyticus*, however, no entire *sxs*A open-reading frame was found for this organism, as the sequence is split on different contigs in the few genomes in which it is encoded. Therefore, *S. saprophyticus* was not included in any of the further analyses. A higher number of hits and entirely encoded gene sequences were found for certain *Staphylococcus cohnii* isolates. In *S. cohnii*, however, *sxs*A is not part of the core genome, as it was only identified in a small group of strains, all isolated from a dairy environment/bovine mastitis infection (either SNUC strains originating from Canada or SC strains, originating from Germany). When considering a recent taxonomic revision published by Lavecchia et al. (2021), which revealed three phylogenetically distinct lines within *S. cohnii*, *sxs*A-positive isolates all correspond to group A2, a group proposed by the authors to be reclassified to *Staphylococcus cohnii* subsp. *barensis*. *Sxs*A would therefore join the list of strain-specific genes of this subspecies. Whether *sxs*A was acquired by *S. cohnii* due to horizontal gene transfer is not clearly evident. An identical shared gene synteny was found in all staphylococcal species analyzed (Figure S7). *Sxs*A is surrounded by the same set of genes, moreover, no indicators for a localization on a mobile genetic element were identifiable as no flanking transposases, integrases, recombinases, or plasmid-associated genes are located nearby. Furthermore, computational genomic island finders did not yield any hits for this region either. Thus, it appears that *sxs*A is part of the chromosome in a region with low plasticity, at least in those species in which it is part of the core genome, and it remains open whether *Staphylococcus cohnii* subsp. *barensis* has acquired the gene exogenously during speciation or if other *S. cohnii* have lost it during evolution.

3.8 | Primary sequence organization of SxsA

Domain structure analysis of SxsA was made based on the alignment of 44 different SxsA sequences, originating from four different staphylococcal species, and subsequent analysis of conserved regions and secondary structure (alpha and beta structures, coiled-coil motifs, amyloidogenic regions). Only complete open-reading frames, entirely encoded on one contig, were considered. Table S5 lists all organisms that were included in the analysis. Similar analysis of the SxsA sequences revealed a clear grouping into four different subgroups at a cutoff level of about 16% (see phylogenetic tree provided in Figure S8). This grouping partly reflects the phylogenetic relationship, as sequences of *S. cohnii* and *S. nepalensis* cluster as distinct. The two remaining groups, however, contain both *S. xylosus* and *S. pseudoxylosus* sequences.

SxsA structure can be divided into four domains, as shown in Figure 5, and as described exemplarily for TMW 2.1523 in the following. After the N-terminal signal peptide (YSIRK-G/S, 43 aa), a 286 aa long sequence follows (aa 44–329), which is rich in α-helix structure and predicted to fold into coiled-coil domains from aa 131 to 158 (Figure 5a,b). This region is designated as Region A. Of note is that some strains carry a SxsA version with short-sequence stretches that share >80% similarity with calcium-binding EF-hand motifs in their Region A (marked as a black arrow in Figure S8). Region B (aa 330–520) is rich in β-sheet secondary structure and is the most conserved region of the protein across species (Figure 5b,e). It is also the region of the protein which was computed to carry amyloidprone peptide stretches (Figure 5c). Other YSIRK-G/S, LPxTG-containing staphylococcal surface proteins, such as Bap and Aap, have been shown to mediate biofilm formation by adopting an amyloid conformation (Taglialegna, Navarro, et al., 2016b; Yarawsky et al., 2020). Therefore, special emphasis was led on the prediction and analysis of potential amyloidprone regions for SxsA as well. Similar to Bap and Aap, the amyloidogenic regions of SxsA are located within β-sheet-rich regions of the protein. Comparison of the predicted (by at least three of the four algorithms used) amino acid sequences revealed two short, conserved peptide stretches that display high amyloidogenic potential and which are present in all SxsA sequences analyzed namely $_{455}$LGYYSY$_{460}$ and $_{500}$LFGYILS$_{506}$ (aa positions are indicated for strain TMW 2.1523). Further, *S. xylosus*, *S. pseudoxylosus*, and *S. nepalensis* share a conserved amyloidogenic peptide $_{402}$VLIATMVL$_{409}$ as well as *S. nepalensis* and *S. cohnii* sequences both contain the amyloidprone segment $_{486}$VKFYISFDA$_{494}$ (S. *nep*_JS1) and *S. xylosus* and *S. pseudoxylosus* $_{482}$EFVISFDASYYI$_{493}$ (see Figure 5d and Figure S10, respectively). When referring to amyloid formation, the isoelectric point (pI) is another important parameter to consider as it is assumed that peptide assembly into amyloidogenic structures is enhanced when the environment reaches pH values close to the pI of the peptide (Taglialegna, Navarro, et al., 2016b). While the pI of the entire protein is reached

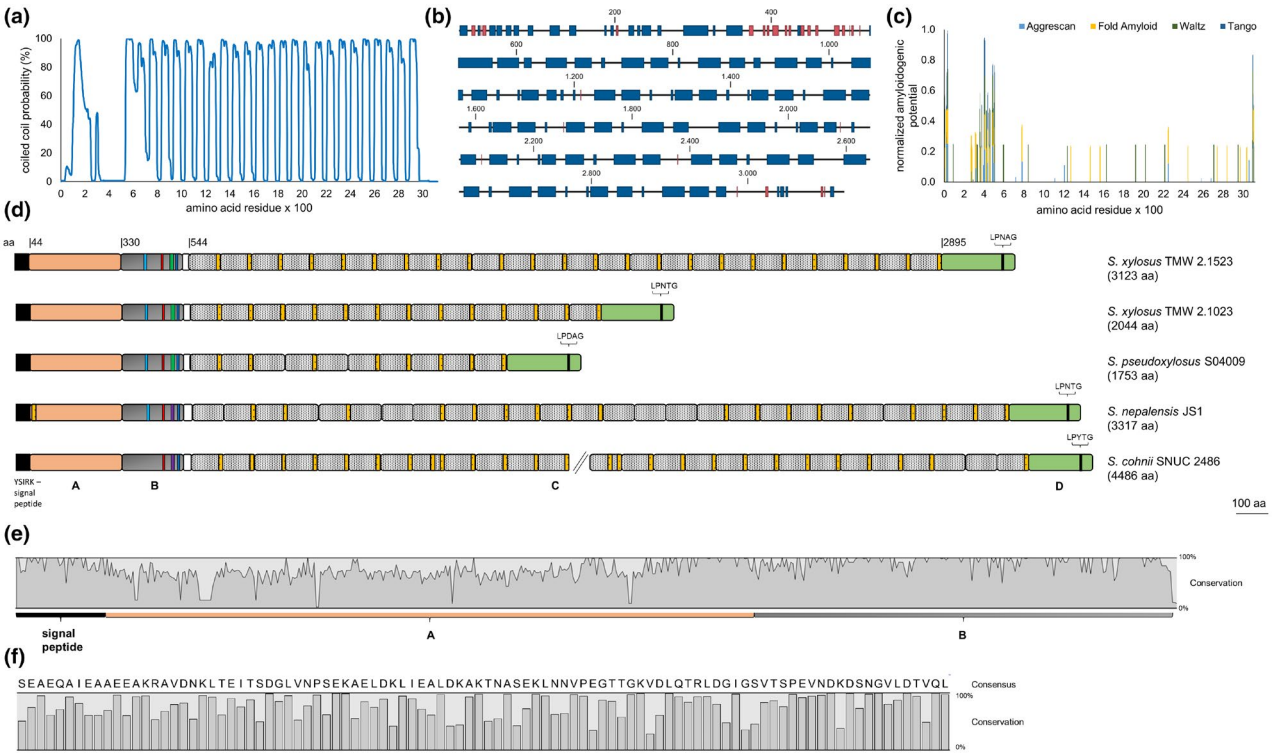

FIGURE 5 Structural organization of SxsA. (a) Prediction of coiled-coil regions (2.1523-SxsA) by MARCOIL. (b) 2.1523-SxsA secondary structure prediction, regions predicted to fold into α-helices and β-sheet are marked in blue and red, respectively. (c) Predicted amyloidogenic potential of 2.1523-SxsA. Columns represent the normalized amyloidogenic potential of SxsA by four different algorithms as Aggrescan (bright blue), FoldAmyloid (yellow), WALTZ (green), and TANGO (blue). (d) SxsA structure of four different staphylococcus species. Signal peptide, cell wall-anchor, and Regions A–D of the protein are displayed as indicated. EF-hand motifs (≥80% similarity) are shown in yellow, conserved amino acid sequences of Region B corresponding to amyloid prone peptides predicted by at least three of the algorithms used are LGYYSY (red), LFGYILS (blue), EFVISFDASYYI (green), VKFYISFDA (violet), and VLIATMVL (bright blue). SxsA of *S. cohnii* SNUC 2486 harbors 40 repeats in its C-region of which not all are shown due to space restrictions. (e) Conservation plot of the N-terminal part of the protein (SP, Regions A and B) when SxsA of 44 different strains is aligned with MUSCLE. (f) Conservation and consensus sequence when all C-repeats of all 44 analyzed SxsA sequences are aligned

under acidic conditions (4.4–4.8), the pI of SxsA Region B only is reached in the basic milieu (pI values around 8.0–9.1).

Region B is followed by a short spacer sequence after which Region C starts. Region C consists of 98 aa long repeats, not identical in their sequence but with some conserved amino acids (Figure 5f). SxsA varies in the number of repeats not only between but also within staphylococcal species. In the here performed analysis, the lowest number (4) of repeats was found in *S. xylosus* SNUC233 and the highest number (44) in *S. nepalensis* NCTC10517 and *S. xylosus* DMSX03 (Table S5). The different number of repeats is the main reason for the varying length/molecular weight of the protein among different strains. The C-repeats are further predicted to fold into coiled-coil motifs and almost every repeat sequence harbors a motif that shares more than 80% similarity with the loop consensus of Ca^{2+}-binding EF-hand motifs (Lewit-Bentley & Réty, 2000). Region D (aa 2895–3123) is at the C-terminal part of the protein and includes the LPxTG cell wall-anchor domain as well as the characteristic hydrophobic amino acid segment, often found in surface proteins with an LPxTG motif. In contrast to Bap (Cucarella et al., 2001; Schiffer et al., 2019), no repeats are identifiable in Region D of SxsA nor are serine and aspartic acid residues (SD repeats) present in any of the SxsA Region D sequences.

SxsA of all analyzed organisms shares the same structural characteristics described in this section. Coiled-coil formation, amyloidogenic potential, as well as secondary structure prediction for *S. xylosus* TMW 2.1023, *S. nepalensis* JS1, *S. pseudoxylosus* S04009, and *S. cohnii* SNUC2486 are shown in Figure S10. An overview of structural organization, number of C-repeats, and number of EF-hand motifs are provided by Figure S9.

3.9 | Microscopic analysis of biofilm matrix and cell morphology

As the phenotype of Δ*sxs*A was more distinct in TMW 2.1523 in the previously described experiments, it was decided to perform microscopic analyses with this strain and its respective *sxs*A mutants

in TSB_N, only. Microscopic analysis (CLSM and SEM) confirmed the different aggregation behavior of wildtype and *sxs*A-mutant strains. In contrast to thin layers of homogenously distributed mutant cells (single and double mutant), the wildtype strain formed compact, multilayered biofilms with densely packed cell aggregates and adhered well to the surface of porous glass beads (Figure 6a,b). Thereby, it

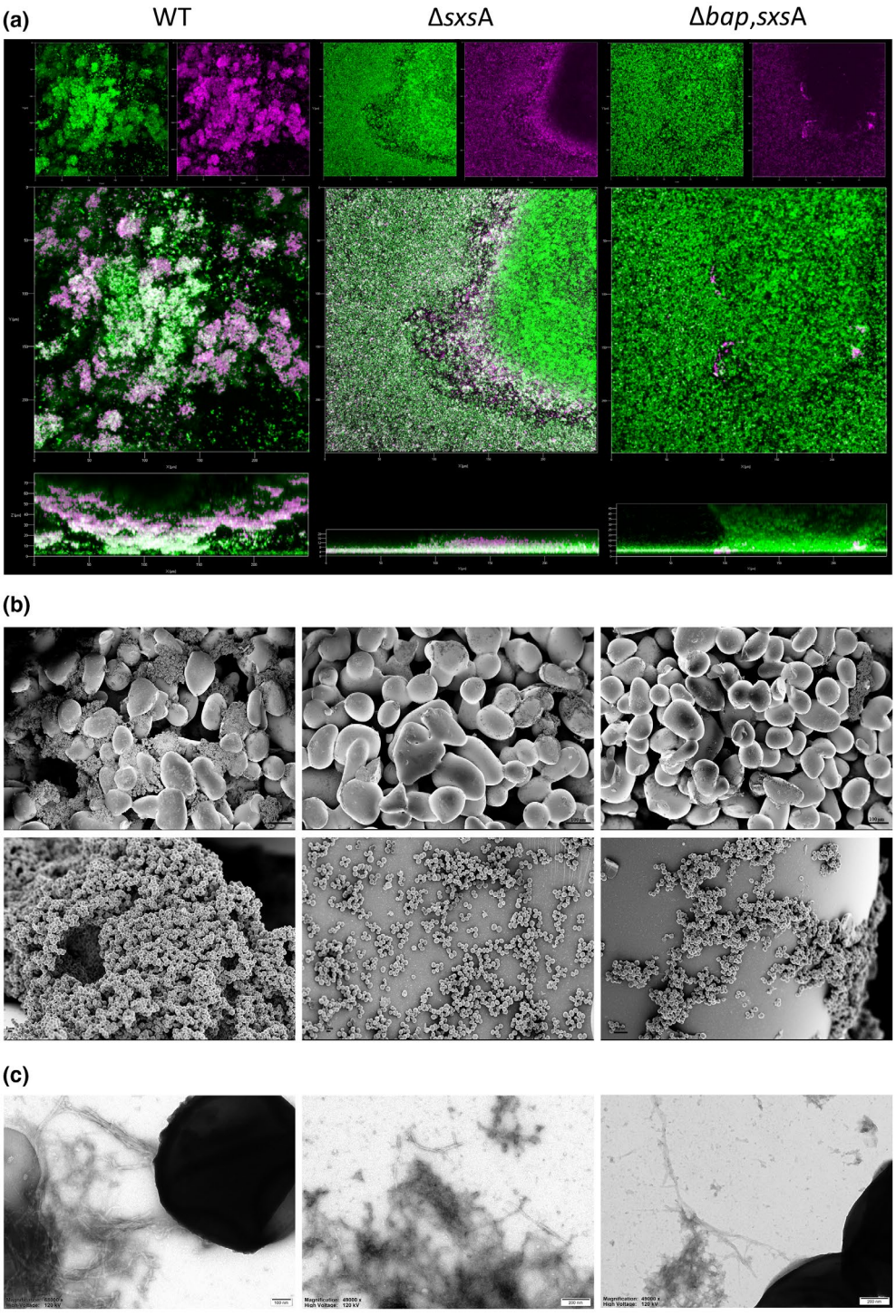

FIGURE 6 Microscopic analysis *S. xylosus* TMW 2.1523 wildtype and mutant biofilms. (a) Confocal laser scanning microscopy of *S. xylosus* TMW 2.1523 wildtype and *sxs*A single- and double-mutant biofilms/cell aggregates after 16 h of incubation (TSB_N, 150 rpm). Staining was performed using Thioflavin T (green) and Syto60 (violet). Top view single-channel images are shown on the top, the respective merged view in the middle, and merged profile (vertical) views below. (b) Scanning electron microscopy of cell aggregates adherent to porous glass beads after 16 h of incubation (TSB_N, 150 rpm). Bacteria were subjected to shear forces during incubation (150 rpm). Two different magnitudes are shown (250x, 5kx). (c) Negative-stained transmission electron micrographs to visualize fibrillar structures of *S. xylosus* cells grown for 16 h (TSB_N, 180 rpm). Scale bars are included in the figure and labeled accordingly

formed a thick biofilm layer even on the outer parts of the beads that were subjected to high shear forces during incubation.

Since literature research, bioinformatic analyses as well as preliminary results from congo red agar plates indicated that the *S. xylosus* biofilm matrix consists of amyloid fibers and that SxsA might contribute to such fiber formation, microscopic analyses were also used to further investigate the composition and structure of *S. xylosus* wildtype and mutant biofilm matrices. Amyloids are protein aggregation disorders that are often found as a structural component in biofilm matrices to provide integrity. Thioflavin T (ThT) is a fluorescent dye commonly used to stain amyloid fibrils. We found that generally large parts of the *S. xylosus* biofilm matrix responded to ThT staining (Figure 7a). Interestingly, regions responding solely to ThT staining were observed in mutant strains while in wildtype samples, most structures responded to both stains, indicating a mixture of DNA (cells/eDNA, stained by nucleic acid stain Syto60) and amyloidogenic structures (ThT staining). SEM analysis confirmed that *sxs*A mutants formed less-adherent biofilm, especially not on surfaces exposed to high shear forces, with only very few parts of the culture assembling to multicellular aggregates (Figure 6b). TEM analysis revealed the presence of at least two different fiber types surrounding the cells, which were often embedded in a slimy kind of matrix (Figure 6c). Yet again, such thin and thick fibers as well as the slimy matrix were detectable in all three sample types. All in all, microscopic analysis confirmed the presence of fibrillar structures in *S. xylosus* TMW 2.1523 biofilms. At least parts of these fibrillar structures are probably of an amyloidogenic nature since highly fluorescent complexes were visible upon ThT staining. Differences between wildtype and mutant, however, were only ascribable to their aggregation and surface adherence behavior and not to fiber type, amount, or ThT staining intensities.

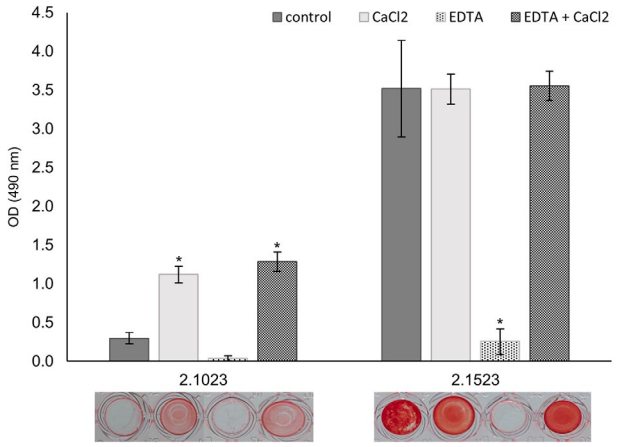

FIGURE 7 Influence of calcium on biofilm formation of *S. xylosus*. Biofilm formation was quantified in 96-well plates (hydrophobic support). Therefore, cells were incubated in TSB_N for a period of 24 h. Either 20 mM $CaCl_2$, 0.2 mM EDTA, or both reagents were added to the wells at the beginning of the incubation period

3.10 | Importance of calcium on biofilm formation of *S. xylosus*

EF-hand motifs, which bioinformatic analysis predicted to occur multiple times in the sequence of SxsA, are known to bind divalent cations such as Ca^{2+}. Such binding of cations to EF-hand motifs of proteins has been previously shown to modulate protein conformation and regulate assembly (Lewit-Bentley & Réty, 2000; Taglialegna, Navarro, et al., 2016b). Therefore, we investigated the influence of calcium on biofilm formation of *S. xylosus*. Wildtype strains TMW 2.1023 and TMW 2.1523 were screened for adhesive biofilm formation in a 96-well-based assay, this time $CaCl_2$ was added in the presence or absence of its respective chelator ethylenediaminetetraacetic (EDTA). As shown in Figure 7, biofilm formation was either unaffected or significantly enhanced when calcium was added, a result especially prevalent in strain TMW 2.1023. The addition of EDTA (0.2 μM) completely abolished biofilm formation in both strains, an effect that could be restored by adding sufficient amounts of calcium again (200 mM).

4 | DISCUSSION

Over the past years, many cell wall-anchored (CWA) proteins of *S. aureus* and *S. epidermidis* have been functionally characterized and current knowledge on staphylococcal biofilm formation is mainly based on the results obtained for these two prominent species (Foster, 2020; Foster et al., 2014; Speziale et al., 2014). Little research has been done on biofilm formation of other CNS such as *S. xylosus*, except for some valuable studies on *S. xylosus* strain C2a, focusing on the eDNA part of biofilm matrices though (Leroy et al., 2021; Planchon et al., 2006). Since the matrix composition of biofilms and mechanisms of adherence are complex and variable among staphylococci, including other species in the research will help to provide a more comprehensive picture. This is particularly relevant when considering that biofilm-mediating genes can easily migrate from CNS into highly pathogenic species such as reported for Bap into bovine strains of *S. aureus* (Tormo et al., 2005).

We have recently published that biofilm-forming mechanisms investigated for one staphylococcal species cannot easily be applied to other species, as we have shown that Bap is not conferring biofilm formation in *S. xylosus* to the same extent as it does in *S. aureus* (Schiffer et al., 2021). To our knowledge, we here present the first data of a newly discovered surface protein, occurring in *S. xylosus* and related species, which is involved in intercellular aggregation and adhesive biofilm formation on surfaces.

SxsA is a large, cell wall-anchored protein (TMW 21023: 223 kDa, TMW 21523: 338 kDa), displaying little sequence identity with other well-known staphylococcal surface proteins, yet sharing a very similar structural organization with CWA proteins such as Bap, the biofilm homologous protein Bhp, and *S. aureus* surface protein SasC (Cucarella et al., 2001; Foster, 2020; Schroeder et al., 2009; Tormo et al., 2005). Like other CWA proteins, SxsA is

organized into domains, where the N-terminal signal peptide is followed by no repeats containing sequence stretches, Regions A and B, of which Region B is highly conserved among SxsA of different species. Region B is also the part of the protein which mainly folds into β-sheet structures and which is predicted to possess high amyloidogenic potential. The core region of the protein is composed of varying numbers of imperfect tandem repeats (C-repeats) followed by the C-terminal Region D which contains the LPxTG motif, a typical cell wall anchor of staphylococcal surface adhesions (Bowden et al., 2005; Speziale et al., 2014). Region D of staphylococcal surface adhesions is often rich in SD repeats (Bowden et al., 2005), this is, however, not applicable to SxsA. The role of C-repeats in bacterial surface proteins has been controversially discussed in the past. From homophilic interactions of repeating structures on neighboring cells over immune evasion mechanisms to structural roles by maintaining proper protein conformation and/or projecting N-terminal ligand-binding domains from the cell surface up to no functional role in the molecular mechanism of biofilm formation at all (Cucarella et al., 2004; Rohde et al., 2007; Valle et al., 2012). Which function C-repeats of SxsA have, and whether the coiled-coil structure contributes to multicellular behavior remains to be discovered. Based on the data presented in the literature for other CWA proteins and the experiments conducted in this study, another mechanism of SxsA-conferring biofilm formation seems to be just as likely though. Instead of the usually extensive core region of CWA proteins, the N-terminal part of staphylococcal surface proteins is often rather substantial in the adhesion and biofilm accumulation process. Many surface adhesions display ligand-binding regions in their N-terminal part (Foster, 2019). Additionally, many CWA proteins have been shown to form amyloidogenic fibers after extracellular processing of the N-terminal part of the protein and thereby contribute to the structural integrity of biofilms (Erskine et al., 2018; Foster, 2020; Taglialegna, Lasa, et al., 2016a). The exact mechanisms of amyloid assembly differ between biofilm proteins, though. Bap and the enterococcal surface protein Esp, for instance, form amyloidogenic fibers through self-assembly of released amyloidprone peptides (Taglialegna, Navarro, et al., 2016b), while Aap-based functional amyloid fibers originate from interactions of exposed repeat-containing domains on the cell surface in the presence of Zn^{2+} (Yarawsky et al., 2020). A high potential to fold into amyloidogenic structures is predicted for Region B of SxsA as well, and red phenotypes on CRA provided a promising first indicator. The additional microscopic analysis confirmed the presence of fibers, likely of an amyloidogenic nature, in *S. xylosus* biofilms. Yet, no clear differences between wildtype and mutants were detectable in this regard. This does not necessarily mean that SxsA is not contributing to amyloid fiber formation, it rather emphasizes the multifactorial nature of *S. xylosus* biofilm formation. Furthermore, the influence of metal ions on *sxs*A-mediated biofilm formation can only be speculated at this timepoint. Divalent ions play important parts in the amyloidogenesis of peptides and protein-based cell aggregation of bacteria. Zn^{2+}, for example, has been shown to be essential for Aap- and SasG-mediated cell aggregation (Geoghegan et al., 2010; Yarawsky et al., 2020). Ca^{2+}, on the other hand, is known for inhibiting Bap-mediated biofilm formation in *S. aureus* (Arrizubieta et al., 2004). This inhibitory effect relies on the binding of the ion to EF-hand motifs in the amyloid-prone region of the protein (Taglialegna, Navarro, et al., 2016b). We have previously shown that biofilm formation of *S. xylosus* is not inhibited by Ca^{2+} addition to the growth medium but rather enhanced (Schiffer et al., 2021). Here we prove that calcium is essential for biofilm formation of *S. xylosus*, as the addition of the ion significantly enhanced adherence of TMW 2.1023 to polystyrene plates and EDTA completely abolished biofilm formation of both *S. xylosus* strains. Thus, even though SxsA carries many EF-hand motifs, an inhibiting effect of the ion through binding to EF-hand motifs and stabilization of the molten globule state thereby preventing self-assembly into amyloid fibers, can be excluded (Taglialegna, Navarro, et al., 2016b). On the contrary, we suggest that calcium rather mediates interactions of *S. xylosus* surface proteins, maybe even by interacting with SxsA, in a similar way as it is described for Aap and zinc (Conrady et al., 2008).

In this study, we found SxsA to influence multicellular behavior and adhesion to abiotic surfaces in a strain-specific manner. Biofilm formation in the 96-well assay was completely disrupted upon deletion of SxsA in *S. xylosus* strain TMW 2.1523 while it was only impaired in TMW 2.1023. This corroborates the complexity of biofilm formation in staphylococci and the high variability of mechanisms between strains. In this context, it is worth mentioning that the genetic background of the two strains is different. TMW 2.1023 carries a plasmid, encoding another CWA protein (SxsB) which shares typical characteristics of biofilm-associated surface proteins and could therefore compensate for the loss of SxsA or mask the effect in the first place. However, it might just as well be possible that the mechanism of biofilm formation in TMW 2.1023 is a completely different one and that it rather relies on other factors such as eDNA or a yet unidentified polysaccharide. Here one should also keep in mind that biofilm formation in TMW 2.1023 is generally lower than in TMW 2.1523 and while the latter tends to autoaggregate heavily, TMW 2.1023 shows no visible cell aggregation in TSB_N and only little in TSB^+.

It is known that staphylococcal biofilm matrices consist of proteins, eDNA, and polysaccharides in different proportions (Schilcher & Horswill, 2020). Our data once again demonstrate that differences in number, nature, and impact of proteinaceous components involved exist between different species and even different strains.

*Sxs*A is encoded in a group of staphylococci that have all been associated with mastitis infections in the past (Condas et al., 2017; de Buck et al., 2021). However, the potential role of SxsA in adhesion to biotic surfaces (intramammary adherence), infectious processes, and subordinate effects of biofilm formation (e.g., antimicrobial susceptibility) can currently only be speculated. Further studies on molecular mechanisms of *sxs*A-mediated biofilm formation and the role of the protein during infections are warranted.

In conclusion, this study describes a novel staphylococcal surface protein-mediating intercellular adhesion and promoting biofilm formation on abiotic surfaces.

ACKNOWLEDGMENTS

Part of this work was funded by the German Federal Ministry for Economic Affairs and Energy via the German Federation of Industrial Research Associations (AiF) and the Forschungskreis der Ernährungsindustrie E.V. (FEI), project AiF 19690 N. Open Access funding enabled and organized by Projekt DEAL.

CONFLICT OF INTEREST

The authors received a research grant from the AiF, which did not influence the aims or setup of this study, and declare no conflict of interest.

AUTHOR CONTRIBUTIONS

Carolin J. Schiffer: conceptualization, data acquisition, analysis, and interpretation, writing—original draft preparation; Christoph Schaudinn: data acquisition and analysis, writing—review and editing; Matthias A. Ehrmann: conceptualization, data analysis and interpretation, supervision, writing—review and editing; Rudi F. Vogel: funding acquisition, project administration, supervision, writing—review and editing.

DATA AVAILABILITY STATEMENT

Whole genome sequencing data of TMW 2.1023 and TMW 2.1523 have been deposited at GenBank under the accessions JAEMUG000000000 and CP066721-CP066725, respectively. The proteomics dataset is accessible via ProteomeXchange using the identifier PXD029728.

REFERENCES

Arrizubieta, M.J., Toledo-Arana, A., Amorena, B., Penadés, J.R. & Lasa, I. (2004) Calcium inhibits Bap-dependent multicellular behavior in *Staphylococcus aureus*. *Journal of Bacteriology*, *186*(22), 7490–7498. Available from: https://doi.org/10.1128/JB.186.22.7490-7498.2004

Bai, Q., Ma, J., Zhang, Z., Zhong, X., Pan, Z., Zhu, Y. et al. (2020) YSIRK--G/S-directed translocation is required for *Streptococcus suis* to deliver diverse cell wall anchoring effectors contributing to bacterial pathogenicity. *Virulence*, *11*(1), 1539–1556. Available from: https://doi.org/10.1080/21505594.2020.1838740

Becker, K., Heilmann, C. & Peters, G. (2014) Coagulase-negative staphylococci. *Clinical Microbiology Reviews*, *27*(4), 870–926. Available from: https://doi.org/10.1128/CMR.00109-13

Bertelli, C., Laird, M.R., Williams, K.P., Lau, B.Y., Hoad, G., Winsor, G.L. et al. (2017) IslandViewer 4: expanded prediction of genomic islands for larger-scale datasets. *Nucleic Acids Research*, *45*(W1), W30–W35. Available from: https://doi.org/10.1093/nar/gkx343

Bowden, M.G., Visai, L., Longshaw, C.M., Holland, K.T., Speziale, P. & Hook, M. (2002) Is the GehD lipase from *Staphylococcus epidermidis* a collagen binding adhesin? *The Journal of Biological Chemistry*, *277*(45), 43017–43023. Available from: https://doi.org/10.1074/jbc.M207921200

Bowden, M.G., Chen, W., Singvall, J., Xu, Y., Peacock, S.J., Valtulina, V. et al. (2005) Identification and preliminary characterization of cell-wall-anchored proteins of *Staphylococcus epidermidis*. *Microbiology (Reading, England)*, *151*(Pt 5), 1453–1464. Available from: https://doi.org/10.1099/mic.0.27534-0

de Buck, J., Ha, V., Naushad, S., Nobrega, D.B., Luby, C., Middleton, J.R. et al. (2021) Non-aureus staphylococci and bovine udder health: current understanding and knowledge gaps. *Frontiers in Veterinary Science*, *8*, 658031. Available from: https://doi.org/10.3389/fvets.2021.658031

Condas, L.A.Z., de Buck, J., Nobrega, D.B., Carson, D.A., Roy, J.-P., Keefe, G.P. et al. (2017) Distribution of non-aureus staphylococci species in udder quarters with low and high somatic cell count, and clinical mastitis. *Journal of Dairy Science*, *100*(7), 5613–5627. Available from: https://doi.org/10.3168/jds.2016-12479

Conrady, D.G., Brescia, C.C., Horii, K., Weiss, A.A., Hassett, D.J. & Herr, A.B. (2008) A zinc-dependent adhesion module is responsible for intercellular adhesion in staphylococcal biofilms. *Proceedings of the National Academy of Sciences*, *105*(49), 19456–19461. Available from: https://doi.org/10.1073/pnas.0807717105

Cucarella, C., Solano, C., Valle, J., Amorena, B., Lasa, I. & Penadés, J.R. (2001) Bap, a *Staphylococcus aureus* surface protein involved in biofilm formation. *Journal of Bacteriology*, *183*(9), 2888–2896. Available from: https://doi.org/10.1128/JB.183.9.2888-2896.2001

Cucarella, C., Tormo, M.A., Ubeda, C., Trotonda, M.P., Monzon, M., Peris, C. et al. (2004) Role of biofilm-associated protein Bap in the pathogenesis of bovine *Staphylococcus aureus*. *Infection and Immunity*, *72*(4), 2177–2185. Available from: https://doi.org/10.1128/IAI.72.4.2177-2185.2004

Decker, R., Burdelski, C., Zobiak, M., Büttner, H., Franke, G., Christner, M. et al. (2015) An 18 kDa scaffold protein is critical for *Staphylococcus epidermidis* biofilm formation. *PLOS Pathogens*, *11*(3), e1004735. Available from: https://doi.org/10.1371/journal.ppat.1004735

DeDent, A., Bae, T., Missiakas, D.M. & Schneewind, O. (2008) Signal peptides direct surface proteins to two distinct envelope locations of *Staphylococcus aureus*. *The EMBO Journal*, *27*(20), 2656–2668. Available from: https://doi.org/10.1038/emboj.2008.185

Delorenzi, M. & Speed, T. (2002) An HMM model for coiled-coil domains and a comparison with PSSM-based predictions. *Bioinformatics (Oxford, England)*, *18*(4), 617–625. Available from: https://doi.org/10.1093/bioinformatics/18.4.617

Erskine, E., MacPhee, C.E. & Stanley-Wall, N.R. (2018) Functional amyloid and other protein fibers in the biofilm matrix. *Journal of Molecular Biology*, *430*(20), 3642–3656. Available from: https://doi.org/10.1016/j.jmb.2018.07.026

Fernandez-Escamilla, A.-M., Rousseau, F., Schymkowitz, J. & Serrano, L. (2004) Prediction of sequence-dependent and mutational effects on the aggregation of peptides and proteins. *Nature Biotechnology*, *22*(10), 1302–1306. Available from: https://doi.org/10.1038/nbt1012

Foster, T.J. (2019) The MSCRAMM family of cell-wall-anchored surface proteins of gram-positive cocci. *Trends in Microbiology*, *27*(11), 927–941. Available from: https://doi.org/10.1016/j.tim.2019.06.007

Foster, T.J. (2020) Surface proteins of *Staphylococcus epidermidis*. *Frontiers in Microbiology*, *11*, 1829. Available from: https://doi.org/10.3389/fmicb.2020.01829

Foster, T.J., Geoghegan, J.A., Ganesh, V.K. & Höök, M. (2014) Adhesion, invasion and evasion: the many functions of the surface proteins of *Staphylococcus aureus*. *Nature Reviews Microbiology*, *12*(1), 49–62. Available from: https://doi.org/10.1038/nrmicro3161

Gabler, F., Nam, S.-Z., Till, S., Mirdita, M., Steinegger, M., Söding, J. et al. (2020) Protein sequence analysis using the MPI bioinformatics toolkit. *Current Protocols in Bioinformatics*, *72*(1), e108. Available from: https://doi.org/10.1002/cpbi.108

Garbuzynskiy, S.O., Lobanov, M.Y. & Galzitskaya, O.V. (2010) FoldAmyloid: a method of prediction of amyloidogenic regions from protein sequence. *Bioinformatics (Oxford, England)*, *26*(3), 326–332. Available from: https://doi.org/10.1093/bioinformatics/btp691

Geoghegan, J.A., Corrigan, R.M., Gruszka, D.T., Speziale, P., O'Gara, J.P., Potts, J.R. et al. (2010) Role of surface protein SasG in biofilm

formation by *Staphylococcus aureus*. *Journal of Bacteriology*, *192*(21), 5663–5673. Available from: https://doi.org/10.1128/JB.00628-10

de Groot, N.S., Castillo, V., Graña-Montes, R. & Ventura, S. (2012) AGGRESCAN: method, application, and perspectives for drug design. *Methods in Molecular Biology (Clifton, N.J.)*, *819*, 199–220. Available from: https://doi.org/10.1007/978-1-61779-465-0_14

Heilmann, C., Hussain, M., Peters, G. & Götz, F. (1997) Evidence for autolysin-mediated primary attachment of *Staphylococcus epidermidis* to a polystyrene surface. *Molecular microbiology*, *24*(5), 1013–1024. Available from: https://doi.org/10.1046/j.1365-2958.1997.4101774.x

Karatan, E. & Watnick, P. (2009) Signals, regulatory networks, and materials that build and break bacterial biofilms. *Microbiology and Molecular Biology Reviews*, *73*(2), 310–347. Available from: https://doi.org/10.1128/MMBR.00041-08

Lavecchia, A., Chiara, M., de Virgilio, C., Manzari, C., Pazzani, C., Horner, D. et al. (2021) Comparative genomics suggests a taxonomic revision of the *Staphylococcus cohnii* species complex. *Genome Biology and Evolution*, *13*(4), 1–14. Available from: https://doi.org/10.1093/gbe/evab020

Lawal, O.U., Barata, M., Fraqueza, M.J., Worning, P., Bartels, M.D., Goncalves, L. et al. (2021) *Staphylococcus saprophyticus* from clinical and environmental origins have distinct biofilm composition. *Frontiers in Microbiology*, *12*, 663768. Available from: https://doi.org/10.3389/fmicb.2021.663768

Leroy, F., Verluyten, J. & Vuyst, L.D. (2006) Functional meat starter cultures for improved sausage fermentation. *International Journal of Food Microbiology*, *106*(3), 270–285. Available from: https://doi.org/10.1016/j.ijfoodmicro.2005.06.027

Leroy, S., Lebert, I., Andant, C., Micheau, P. & Talon, R. (2021) Investigating extracellular DNA release in *Staphylococcus xylosus* biofilm in vitro. *Microorganisms*, *9*(11), 2192. Available from: https://doi.org/10.3390/microorganisms9112192

Lewit-Bentley, A. & Réty, S. (2000) EF-hand calcium-binding proteins. *Current Opinion in Structural Biology*, *10*(6), 637–643. Available from: https://doi.org/10.1016/S0959-440X(00)00142-1

Louros, N., Konstantoulea, K., de Vleeschouwer, M., Ramakers, M., Schymkowitz, J. & Rousseau, F. (2020) WALTZ-DB 2.0: an updated database containing structural information of experimentally determined amyloid-forming peptides. *Nucleic Acids Research*, *48*(D1), D389–D393. Available from: https://doi.org/10.1093/nar/gkz758

Mazmanian, S.K., Ton-That, H. & Schneewind, O. (2001) Sortase-catalysed anchoring of surface proteins to the cell wall of *Staphylococcus aureus*. *Molecular Microbiology*, *40*(5), 1049–1057. Available from: https://doi.org/10.1046/j.1365-2958.2001.02411.x

Michels, R., Last, K., Becker, S.L. & Papan, C. (2021) Update on coagulase-negative staphylococci-what the clinician should know. *Microorganisms*, *9*(4), 1–13. Available from: https://doi.org/10.3390/microorganisms9040830

Monk, I.R. & Stinear, T.P. (2021) From cloning to mutant in 5 days: rapid allelic exchange in *Staphylococcus aureus*. *Access Microbiology*, *3*(2), 1–7. Available from: https://doi.org/10.1099/acmi.0.000193

Monk, I.R., Shah, I.M., Xu, M., Tan, M.-W. & Foster, T.J. (2012) Transforming the untransformable: application of direct transformation to manipulate genetically *Staphylococcus aureus* and *Staphylococcus epidermidis*. *mBio*, *3*(2), e00277-11. Available from: https://doi.org/10.1128/mBio.00277-11

Otto, M. (2008) Staphylococcal biofilms. *Current Topics in Microbiology and Immunology*, *322*, 207–228.

Planchon, S., Gaillard-Martinie, B., Dordet-Frisoni, E., Bellon-Fontaine, M.N., Leroy, S., Labadie, J. et al. (2006) Formation of biofilm by *Staphylococcus xylosus*. *International Journal of Food Microbiology*, *109*(1-2), 88–96. Available from: https://doi.org/10.1016/j.ijfoodmicro.2006.01.016

Rahmdel, S. & Götz, F. (2021) The multitasking surface protein of *Staphylococcus epidermidis*: accumulation-associated protein (Aap). *mBio*, *12*, e0198921. Available from: https://doi.org/10.1128/mBio.01989-21

Roche, F.M., Massey, R., Peacock, S.J., Day, N.P.J., Visai, L., Speziale, P. et al. (2003) Characterization of novel LPXTG-containing proteins of *Staphylococcus aureus* identified from genome sequences. *Microbiology*, *149*(Pt 3), 643–654. Available from: https://doi.org/10.1099/mic.0.25996-0

Rohde, H., Burdelski, C., Bartscht, K., Hussain, M., Buck, F., Horstkotte, M.A. et al. (2005) Induction of *Staphylococcus epidermidis* biofilm formation via proteolytic processing of the accumulation-associated protein by staphylococcal and host proteases. *Molecular Microbiology*, *55*(6), 1883–1895. Available from: https://doi.org/10.1111/j.1365-2958.2005.04515.x

Rohde, H., Burandt, E.C., Siemssen, N., Frommelt, L., Burdelski, C., Wurster, S. et al. (2007) Polysaccharide intercellular adhesin or protein factors in biofilm accumulation of *Staphylococcus epidermidis* and *Staphylococcus aureus* isolated from prosthetic hip and knee joint infections. *Biomaterials*, *28*(9), 1711–1720. Available from: https://doi.org/10.1016/j.biomaterials.2006.11.046

Schiffer, C., Hilgarth, M., Ehrmann, M. & Vogel, R.F. (2019) Bap and cell surface hydrophobicity are important factors in *Staphylococcus xylosus* biofilm formation. *Frontiers in Microbiology*, *10*, 1387. Available from: https://doi.org/10.3389/fmicb.2019.01387

Schiffer, C.J., Abele, M., Ehrmann, M.A. & Vogel, R.F. (2021) Bap-Independent biofilm formation in *Staphylococcus xylosus*. *Microorganisms*, *9*(12), 2610. Available from: https://doi.org/10.3390/microorganisms9122610

Schilcher, K. & Horswill, A.R. (2020) Staphylococcal biofilm development: structure, regulation, and treatment strategies. *Microbiology and Molecular Biology Reviews*, *84*(3), 1–36. Available from: https://doi.org/10.1128/MMBR.00026-19

Schleifer, K.H. & Kloos, W.E. (1975) Isolation and characterization of staphylococci from human skin I. Amended descriptions of *Staphylococcus epidermidis* and *Staphylococcus saprophyticus* and descriptions of three new species: *Staphylococcus cohnii*, *Staphylococcus haemolyticus*, and *Staphylococcus xylosus*. *International Journal of Systematic Bacteriology*, *25*(1), 50–61. Available from: https://doi.org/10.1099/00207713-25-1-50

Schroeder, K., Jularic, M., Horsburgh, S.M., Hirschhausen, N., Neumann, C., Bertling, A. et al. (2009) Molecular characterization of a novel *Staphylococcus aureus* surface protein (SasC) involved in cell aggregation and biofilm accumulation. *PloS One*, *4*(10), e7567. Available from: https://doi.org/10.1371/journal.pone.0007567

Schuster, C.F., Howard, S.A. & Gründling, A. (2019) Use of the counter selectable marker PheS* for genome engineering in *Staphylococcus aureus*. *Microbiology*, *165*(5), 572–584. Available from: https://doi.org/10.1099/mic.0.000791

Speziale, P., Pietrocola, G., Foster, T.J. & Geoghegan, J.A. (2014) Protein-based biofilm matrices in Staphylococci. *Frontiers in Cellular and Infection Microbiology*, *4*, 171. Available from: https://doi.org/10.3389/fcimb.2014.00171

Supré, K., Haesebrouck, F., Zadoks, R.N., Vaneechoutte, M., Piepers, S. & de Vliegher, S. (2011) Some coagulase-negative Staphylococcus species affect udder health more than others. *Journal of Dairy Science*, *94*(5), 2329–2340. Available from: https://doi.org/10.3168/jds.2010-3741

Taglialegna, A., Lasa, I. & Valle, J. (2016a) Amyloid structures as biofilm matrix scaffolds. *Journal of Bacteriology*, *198*(19), 2579–2588. Available from: https://doi.org/10.1128/JB.00122-16

Taglialegna, A., Navarro, S., Ventura, S., Garnett, J.A., Matthews, S., Penades, J.R. et al. (2016b) Staphylococcal Bap proteins build amyloid scaffold biofilm matrices in response to environmental signals. *PLOS Pathogens*, *12*(6), e1005711. Available from: https://doi.org/10.1371/journal.ppat.1005711

Tormo, M.A., Knecht, E., Götz, F., Lasa, I. & Penades, J.R. (2005) Bap-dependent biofilm formation by pathogenic species of

Staphylococcus: evidence of horizontal gene transfer? *Microbiology (Reading, England)*, *151*(7), 2465–2475. Available from: https://doi.org/10.1099/mic.0.27865-0

Valle, J., Latasa, C., Gil, C., Toledo-Arana, A., Solano, C., Penadés, J.R. et al. (2012) Bap, a biofilm matrix protein of *Staphylococcus aureus* prevents cellular internalization through binding to GP96 host receptor. *PLOS Pathogens*, *8*(8), e1002843. Available from: https://doi.org/10.1371/journal.ppat.1002843

Yarawsky, A.E., Johns, S.L., Schuck, P. & Herr, A.B. (2020) The biofilm adhesion protein Aap from *Staphylococcus epidermidis* forms zinc-dependent amyloid fibers. *Journal of Biological Chemistry*, *295*(14), 4411–4427. Available from: https://doi.org/10.1074/jbc.RA119.010874

Yonemoto, K., Chiba, A., Sugimoto, S., Sato, C., Saito, M., Kinjo, Y. et al. (2019) Redundant and distinct roles of secreted protein eap and cell wall-anchored protein SasG in biofilm formation and pathogenicity of *Staphylococcus aureus*. *Infection and Immunity*, *87*(4), 1–15. Available from: https://doi.org/10.1128/IAI.00894-18

SUPPORTING INFORMATION

Additional supporting information may be found in the online version of the article at the publisher's website.

How to cite this article: Schiffer, C. J., Schaudinn, C., Ehrmann, M. A., & Vogel, R. F. (2022). SxsA, a novel surface protein mediating cell aggregation and adhesive biofilm formation of *Staphylococcus xylosus*. *Molecular Microbiology*, 00, 1–16. https://doi.org/10.1111/mmi.14884